RESEARCH ARTICLE

ADVANCED
PHOTONICS
RESEARCH
Open Access

www.adpr-journal.com

Ultralong Tracking of Fast-Diffusing Nano-Objects inside Nanofluidic Channel—Enhanced Microstructured Optical Fiber

Fengji Gui, Shiqi Jiang, Ronny Förster, Malte Plidschun, Stefan Weidlich, Jiangbo Zhao,* and Markus A. Schmidt*

Nanoparticle tracking analysis (NTA) represents one essential technology to characterize diffusing nanoscale objects. Herein, uncovering dynamic processes and high-precision measurements requires tracks with thousands of frames to reach high statistical significance, ideally at high frame rates. Optical fibers with nanochannels are used for NTA, successfully demonstrating acquisition of trajectories of fast diffusion nano-objects with 100 000 frames. Due to the spatial limitation of the central nanofluidic channel, diffusion of objects illuminated by the core mode is confined, enabling the recording of Brownian motion over extraordinarily long time scales at high frame rates. The resulting benefits are discussed on a representative track of a gold nanosphere diffusing in water in over nearly 100 000 frames at 2 kHz frame rate. In addition to the verification of the fiber-based NTA using two data processing methods, a segmented analysis reveals a correlation between precision of determined diameter and continuous time interval (i.e., number of frames per subtrajectory). The presented results demonstrate the capabilities of fiber-based NTA in terms of 1) determining diameters with extraordinary high precision of single species and 2) monitoring dynamic processes of the object or the fluidic environment, both of which are relevant within biology, microrheology, and nano-object characterization.

1. Introduction

Nanoparticle tracking analysis (NTA) represents a key screening technology within bioanalytics and microrheology to determine the properties of objects or processes at the nanoscale. This approach relies on using the light scattered from the target objects for localization and tracking, with the dimension of the object being deep subwavelength. Examples of NTA applications include biological matters,[1–4] dark-field imaging,[5] multifocal microscopy,[6] and living cell detection.[7]

Within NTA, the length of the recorded trajectory (i.e., the number of frames per track) represents an essential and crucial parameter. First, Brownian motion is statistically analyzed, with the estimated parameters showing improved precision with the number of samples, which in the case here is the number of tracked frames N. For data analysis, the method of mean squared displacement (MSD) is commonly used with the relative error of measurement being limited by the Cramér–Rao lower bound (CRLB), which is proportional to $\approx \sqrt{1/N}$. Moreover, observing the nano-objects over long time scales principally allows to

F. Gui, S. Jiang, Dr. R. Förster, M. Plidschun, Dr. S. Weidlich, Prof. M. A. Schmidt
The Department of Fiber Photonics
Leibniz Institute of Photonic Technologies (IPHT)
Albert-Einstein-Street 9, 07745 Jena, Germany
E-mail: markus.schmidt@leibniz-ipht.de

Dr. S. Weidlich
Research & Development Specialty Fiber Optics
Heraeus Quarzglas GmbH & Co. KG
Quarzstreet 8, 63450 Hanau, Germany

Dr. J. Zhao
Institute for Photonics & Advanced Sensing (IPAS)
School of Physical Sciences
University of Adelaide
Adelaide SA 5005, Australia
E-mail: jiangbo.zhao62@gmail.com

Prof. M. A. Schmidt
Abbe Center of Photonics and Faculty of Physics
Friedrich-Schiller-University Jena
Max-Wien-Platz 1, 07743 Jena, Germany

Prof. M. A. Schmidt
Otto Schott Institute of Materials Research (OSIM)
Friedrich Schiller University Jena
Fraunhoferstr. 6, 07743 Jena, Germany

**ADVANCED
SCIENCE NEWS**

www.advancedsciencenews.com

**ADVANCED
PHOTONICS
RESEARCH**

www.adpr-journal.com

dynamically monitor the diffusion process, thus providing a pathway to reveal either changes of the diffusing object itself or a modification of the environment. This ultimately is essential for the unlocking of dynamic processes in biology and micro-rheology such as the interactions between nano-objects,[1,2] or the measurement of anomalous diffusion.[8,9]

Especially in the case of fast diffusion, tracking a single nano-particle over a large number of frames represents one key challenge in NTA. Current technologies show limitations on this issue, particular in light of the fact that the positions of the objects are not limited to a specific spatial area. Basically, a trajectory ends if the object leaves the field of view (FoV) or the focal plane of the objective, which typically happens after a short time. For example, within a typical FoV of (6×6) μm^2, one can only observe a diffusing object with diffusion coefficient $D = 1 \, \mu m^2 \, s^{-1}$ for 1 s.[10,11] Recently, experimental approaches using axial confinement or tracking with adaptive focus and stage have been reported.[5,10,12] They show that single-particle orbit tracking can support a continuous tracking of 150 000 frames but with a rather small diffusion coefficient of 0.017 $\mu m^2 \, s^{-1}$.[10]

A novel NTA scheme that was introduced by the authors in 2015 relies on microstructured optical fibers that include nano- and microfluidic channels along the entire fiber length, supporting fast, label-free, and long-duration observation of nano-objects.[13] This waveguide-based scheme has opened up the field of fiber-based NTA (fNTA), examples of research including the determination of the full 3D trajectory of diffusing gold nanospheres via evanescent-field scattering position retrieval,[14] the simultaneous evaluation of hundreds of diffusing 40 nm gold particles inside antiresonant hollow core fibers,[15] or the measurement of single-virus diffusion (diameter 19 nm) using nano-bore optical fibers (NBFs).[13,16] The essential advantage of the fNTA approach within the context of acquiring trajectory with a large number of frames is related to the confinement of the object to the nanofluidic channel, that is, the liquid channel region. Specifically, three primary advantages can be identified: 1) high-intensity light-line-type illumination across the entire observation length, 2) persistent occupancy of the nano-object in the focus, and 3) high frame rates due to fast read out because of the reduced FoV along 1D. These combined features suggest fNTA to allow for the acquisition of trajectories with an extraordinary number of frames of fast-diffusing objects, potentially opening up new areas of application for NTA.

In this work, we experimentally demonstrate that through limiting transverse particle diffusion via the nanofluidic channel of an NBF, the fNTA concept enables the recording of nearly 100 000 frame (40.3 s) trajectories of a rapidly diffusing nano-object in water. The corresponding Brownian motion was investigated using power spectral density (PSD) and MSD analysis, the latter showing a correlation between measurement accuracy and continuous recorded time interval (i.e., number of frames per subtrajectory), clearly identifying the advantages of exceptionally long trajectories.

2. Working Principle and Design

The NBF-based fNTA approach relies on the detection of the elastically scattered light of the nano-objects diffusing inside the central nanofluidic channel of the fiber. One of the keys to this approach is the concentric fiber geometry, which contains a doped fiber core and a central nanochannel that can be flexibly filled with the nano-object-doped aqueous suspension (**Figure 1**a). The objects diffusing inside the nanofluidic channel scatter the light of the evanescent field of the fundamental mode (red area in Figure 1a), which is laterally detected by a microscope. This conceptual implement allows recording the Brownian motion of nano-object along the longitudinal direction via a continuous acquisition of individual images.

One common issue within the context of waveguide-based NTA that uses total internal refraction as a light guidance mechanism is the low refractive index (RI) of water, being smaller than that of almost all solid materials ($n_{water} < n_{solid}$). This prevents direct light guidance inside the water-filled channel, therefore demanding to use microstructured claddings. Within this work this issue is circumvented by using the NBF approach: Here, a high-RI region (i.e., optical core) surrounds the central water-filled nanochannel, leading to the formation of evanescent fields inside the nanofluidic channel. From the NTA perspective, this geometric arrangement results in a light-line-like illumination upon the diffusing objects, as the transverse intensity distribution the objects experience is essentially identical at any longitudinal position.[13] Note that due to the extension of the nanofluidic channel along the fiber axis, longitudinal diffusion is essentially unconfined, whereas transverse diffusion is corralled due to the presence of the channel walls.

3. Experimental Section

The NBF used here consisted of a GeO_2-doped silica core (diameter $2b = 3.8 \, \mu m$), with a RI that was slightly higher ($\Delta n \approx 8 \times 10^{-3}$) than that of the pure silica cladding (more details of the nanobore can be found in the study by Schaarschmidt[17]). The center of the core included a hollow nanochannel (diameter $2a = 560 \, nm$) filled with gold nanoparticles dispersed in aqueous solution. This fiber supported a fundamental mode with evanescent fields inside the central channel at the operation wavelength ($\lambda = 532 \, nm$) (simulated mode in Figure 1b). The strong evanescent decay (for water, the penetration depth was 0.1 μm) limited the maximum nanobore diameter. Note that due to its unique modal properties and, compared with other types of microstructured fibers, its comparably simple structure, the NBF was used in a series of experiments, examples including nonlinear plasmonics[18] or fiber-integrated spectroscopy.[19]

The used aqueous solution contained ultrauniform gold nanospheres (average physical diameter $\bar{d}_p = (49.9 \pm 2.2) \, nm$, concentration: 4.2×10^{10} particle ml^{-1}, nano-Composix). The average hydrodynamic diameter was measured in house by a Zetasizer (Malvern) to be $\bar{d}_h = (57 \pm 10) \, nm$ (more details can be found in Supporting Information).

Filling of the nanofluidic channel was conducted through capillary force in minutes by placing the output side of the fiber into the particle solution (**Figure 2**a). After the solution reached the observation area, the output side of the fiber was sealed by a patch of plasticine to prevent further flow, thus eliminating particle drift and allowing the nano-objects to remain within the observation area.
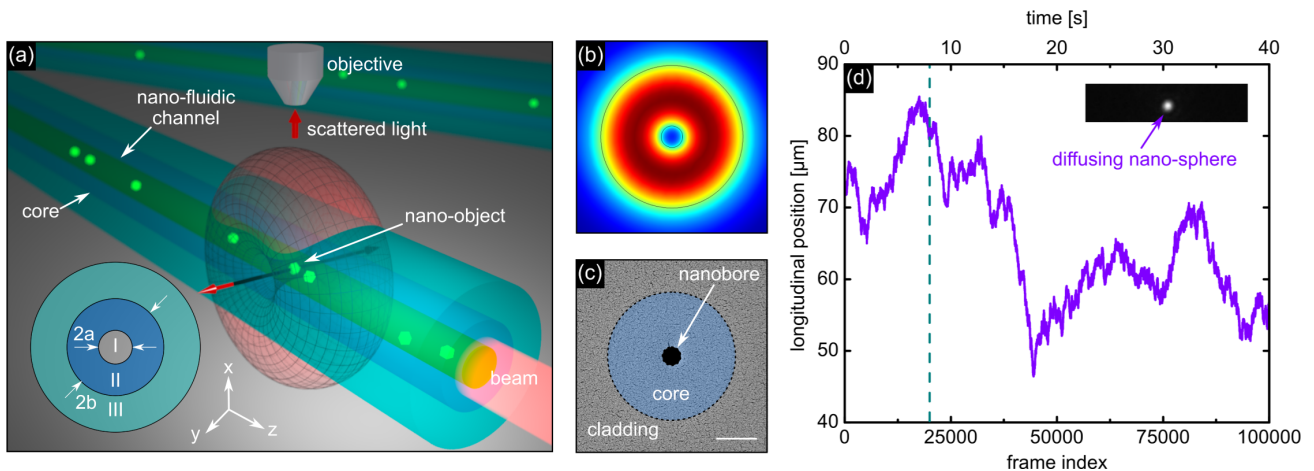
Figure 1. Nano-object tracking inside a nanofluidic channel-enhanced step-index fiber. a) Sketch of the concept, consisting of NBF, nanofluidic channel, diffusing nano-objects, optical mode, and objective. The red area highlights the scattered light of a selected nano-object (the toroidal shape resembles the principle scattering pattern, neglecting the reflection at various interfaces). The inset in the bottom-left corner shows the cross section of the fiber, that is, transverse RI distribution (I: nanofluidic channel, $n_1 = 1.3337$, II: doped core, $n_2 = 1.4687$, III: silica cladding, $n_3 = 1.4607$. b) Simulated spatial intensity distribution (linear scale, dark red: 1; dark blue: 0) of the fundamental mode in case the central nanochannel is filled with water ($\lambda = 532$ nm, geometric and material parameters are given in the text). c) Scanning electron microscopic image of the central section of the NBF (scale bar is 1 μm, bore diameter: 0.56 μm). d) Measured longitudinal trajectory (along the z-axis) of a 53 nm gold nanosphere diffusing in water as a function of frame index (bottom axis) or time (top axis). This track includes a large number of frames ($N_t = 10^5$) and is used as a representative example dataset for the analyses in this work. The vertical dashed dark cyan line shows the maximum trajectory length from our previous NBF work.[13] The inset in the top-right corner shows an example frame of that track (a close-up view of the scattering pattern of the particle can be found in Supporting Information).
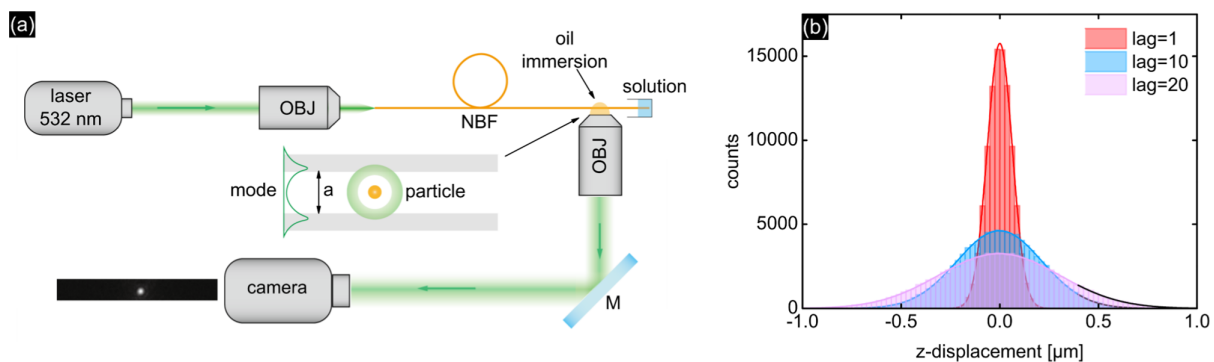

Figure 2. a) Experimental setup used for particle tracking, consisting of mode excitation arrangement, NBF, and microscope. The central inset (not to scale) shows the scattering process including mode pattern and scattered light. The image in the lower left corner shows the measured image of the detected particle in one frame. b) Statistical distribution of the experimental longitudinal displacement shown at three different lag-times (red: lag-time = 1 frame (0.4 ms), blue: lag-time = 10 frames (4 ms), and magenta: lag-time = 20 frames (8 ms)).

For the optical experiments (setup in Figure 2a), green laser light ($\lambda = 532$ nm, WhisperIT, W532-50FS) was coupled into the NBF via an objective (40×, NA = 0.65, Olympus), and the mean flux in the channel was 1.8 W cm^{-2}. The side-wise scattered light from the nano-objects was collected via an oil-immersed objective (60×, NA = 0.9, Olympus) and imaged onto a fast CMOS camera (ANDOR Zyla 4.2 Plus, scale: 72.6 nm/pixel) with an exposure time of $t_e = 0.2$ ms, frame rate and frame duration of $\nu = 2480$ Hz, and $\Delta t = 0.4$ ms, respectively. Note that the imaging system used in this work was diffraction limited and well optimized, as can be seen from the airy pattern of the scattered nano-object (see Supporting Information for more details). The longest trajectory contained 100 000 frames ($N_t = 10^5$) corresponding to an observation time of $T = 40.3$ s. The entire

trajectory that is exemplarily evaluated in the following section (Figure 1d) showed clear Brownian motion-based diffusion, as the statistical distribution of the nanosphere's z-position (three examples of lag-time are shown in Figure 2b) was well fitted for all lag-times by a normal distribution probability density function.[20] Note that the number of nanospheres within the FoV can be estimated through the concentration of the solution (4.2×10^{10} particles ml^{-1}) and the volume in the region of observation ($\pi \cdot (110\ \mu m) \cdot ((560/2)\ nm)^2 \approx 2.7 \times 10^{-11}$ ml), showing that approximately one nanosphere is statistically located within the FoV.

The Python package "Trackpy"[21] (DOI: 10.5281/zenodo.3492186) was used for image processing to measure the scattering intensity and localize the particles' position

in each frame by center of mass (another possible software was PyNTA which was recently released by Faez et al.[22]). We conducted a test with parallel programming with the following result: the total computing time was 287 s: 1) 101 s for reading the tiff stack file from disk; 2) 124 s for parallel particle localization; and 3) 53 s for particle trajectory linking. A trajectory was formed out of the individual positions by a nearest-neighborhood linking. Note that principally a graphics processing unit can be used to further speed up the computation in the future.

4. Data Analysis

To reveal the improvement of the statistics in case of having trajectories with a large number of frames, the hydrodynamic diameter of one gold nanosphere has been determined under various conditions. Here we apply 1D-MSD analysis using the tracked positions along the longitudinal (z-) direction, which is sufficient for the determination of the diffusion coefficient.[23] In addition, the results are confirmed by PSD analysis.

4.1. MSD Analysis

The 1D MSD of a freely diffusing nano-object $\langle z^2 \rangle$ is proportional to the lag-time Δt[23] and given by

$$\langle z(i\Delta t)^2 \rangle = 2D_f i\Delta t + 2\sigma^2 - \frac{2}{3}D_f t_e \qquad (1)$$

Here, the free (unconfined) diffusion constant D_f is determined through the slope of Equation (1). The hydrodynamic diameter d_h is then obtained through the Einstein−Stokes relation $D_f = k_B T/3\pi\eta d_h$ (k_B: Boltzmann constant and η: viscosity at temperature T).[24] $i \in \{1, \ldots, N_c\}$ is the index of the lag-time (N_c: number of continuous frames in a trajectory). The offset of MSD curve is determined by both localization uncertainty and motion blur, where σ refers to the localization uncertainty and t_e to the camera exposure time.

Here, it is important to note that the transverse confinement provided by the nanofluidic channel leads to a confined diffusion[25,26] through an increased viscosity, also hindering the diffusion along the longitudinal direction because of the liquid's high bulk modulus. This effect is included here by the so-called average resistance factor R_{avg}, leading to the corrected diffusion constant $D_c = D_f/R_{avg}$[14,27] (more details on the resistance factor can be found in the Supporting Information and in the study by Jiang[14]).

The error of the fitted slope of the MSD (Equation (1)) defines the precision of the retrieved diffusion D_f and hydrodynamic diameter d_h and depends on the number of frames N_c.[23] Here it is important to note that the standard deviation σ_D of the obtained free diffusion coefficient can only be approximated in the case of motion blur and finite localization error. Michalet and Berglund have shown that the standard deviation of the diffusion σ_D reaches the CRLB[28] in case N_c is sufficiently large and can be approximated by

$$\frac{\sigma_D}{D_f} \gtrsim \sqrt{\frac{2}{(N_c-1)}}(1+2\sqrt{1+2x})^{\frac{1}{2}} \approx \sqrt{\frac{1}{N_c}} \qquad (2)$$

where x is the reduced square localization error ($x = \frac{\sigma^2}{D_f \Delta t} - \frac{t_e}{3\Delta t}$). Equation (2) clearly shows that the precision of the analysis increases with the number of frames over which the particle is tracked.[23,29,30]

4.2. PSD Analysis

In addition to the MSD method, the free diffusion coefficient D_f can also be retrieved by PSD analysis, which relies on fitting the power spectrum of the position of the nano-object in the frequency domain.[31,32] The method is commonly used to analyze the motion of single particles in harmonic potentials (as, e.g., in optical trapping experiments[33]). As there is no restoring force along the longitudinal direction in our experiments, no harmonic potential is present and the respective fitting function reduces to

$$P(f) = |\tilde{Z}(f)|^2 \approx \frac{D_f/2\pi^2}{f_c^2 + f} \qquad (3)$$

with $\tilde{Z}(f)$ being the Fourier transformation of the particle's trajectory $z(t)$ and f_c the corner frequency, which is close to zero in the case of free diffusion. The fitting is based on a maximal likelihood estimation (MLE).[32]

4.3. Simulation

To examine our experimental findings, we simulated the diffusion of particles for a configuration that corresponds to the experimental circumstances for 10^5 frames and evaluated the data similarly to those of the experiments. Here, only diffusion along the fiber axis is considered, which excludes reflections at the liquid/solid boundary and corresponds to free 1D diffusion. The effect of hindered diffusion has been taken into account by directly using the measured value of (corrected) diffusion coefficient D_c. Note that the assumption of a free 1D diffusion solely along the longitudinal direction has been proven experimentally as the determined MSD/lag-time dependence is purely linear and shows no visible sign of saturation. To make statistically relevant statements, we simulated a large number of different trajectories and averaged them appropriately. In the simulation, we applied microsteps ($m = 100$) as introduced in the supplementary in the study by Michalet[29] to model the motion blur within the individual exposure time for the detected particle.

5. Results

Within the first step of the analysis, the representative trajectory shown in Figure 1d ($N_t = 10^5$) is analyzed by both MSD and PSD method to verify the appropriateness of the approaches and validate the consistency of the results (**Figure 3**, links to the source code and the data can be found in the Supporting Information). Fitting the first two lag-times in the MSD by Equation (1) yields a free diffusion coefficient of $D_f^{MSD} = (5.97 \pm 0.04)\ \mu m^2\ s^{-1}$ (Figure 3a). Using the first two lag-times only is optimal for $x \ll 1$ (here: $x = -0.16$), because higher lag-times would contribute more correlated noise than signal to the fit[23]. This value excellently matches with the PSD results ($D_f^{PSD} = (5.98 \pm 0.05)\ \mu m^2\ s^{-1}$,

**ADVANCED
SCIENCE NEWS**

www.advancedsciencenews.com

**ADVANCED
PHOTONICS
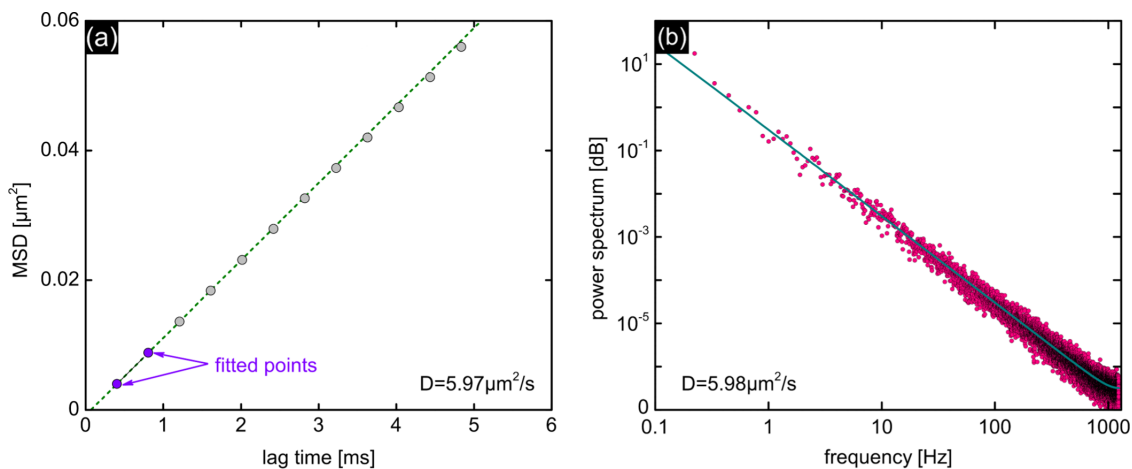RESEARCH** Open Access

www.adpr-journal.com

Figure 3. Data analysis of the entire representative trajectory shown in Figure 1d ($N_t = 10^5$) obtained from a) the 1D MSD analysis and b) the PSD method leading to identical results. In (a), the first two lag-times (purple) have been considered for fitting Equation 2; in (b), the fitting (dark cyan line) was conducted by MLE on the basis of Equation 3.

Figure 3b). The resulting hydrodynamic diameters are $d_h^{MSD} = d_h^{PSD} = (53.3\ 530.6)$ nm, being in the range measured by the Zetasizer ($\bar{d}_h = (57 \pm 10)$ nm).

As shown by Michalet et al.,[23] the finite exposure time (motion blur) leads to a negative offset according to $\mathrm{MSD}_z(t) = 2D_f t - 2D_f t_e/3$, where we assume the localization uncertainty to be negligible compared with the offset term $2D_f t_e/3$. For our experiments, the offset obtained from fitting is $-8.11 \cdot 110^{-16}$ m^2 (entire dataset and $N_{lag} = 2$), which is in agreement with the theoretical prediction ($-2D_f t_e/3 = -7.96 \times 10^{-16}$ m^2). Note that the nanosphere is actually never lost, that is, is present in all frames of the representative dataset, allowing to straightforwardly apply the MSD analysis reported in the study by Jiang et al.[14] (more details can be found in the Supporting Information).

To confirm the merits of having a trajectory with an extremely large number of frames, a segmented MSD analysis of the measured diffusion coefficient has been conducted on the representative trajectory (Figure 1d). Specifically, the entire trajectory is divided into N_s segments of equal length $N_f = N_t/N_s$ which are analyzed separately. As two examples, **Figure 4**a,c shows the time-dependent retrieved-segmented free diffusion coefficient D_f^{seg} in case of 200 and 50 segments with $\approx N_f = 500$ and $N_f = 2000$, respectively. It can be clearly seen that the stable gold nanoparticles' diffusion does not change in time, verifying that fNTA is noninvasive. Both curves indicate that same mean average segmented free diffusion coefficient (obtained from averaging the different values of D_f^{seg}) $\overline{D_f^{seg}} = \frac{1}{N_s} \cdot \sum_j^{N_s} D_f^{seg} = 5.97\ \mu\mathrm{m}^2\,\mathrm{s}^{-1}$ (horizontal magenta lines). Note that, however, the curve in (a) fluctuates more strongly (i.e., has a larger standard deviation σ_D^{seg} marked by the enlarged yellow area) due to the smaller number of frames used in the analyses of the individual subtrajectory N_f. The histograms of the retrieved hydrodynamic diameters are shown in Figure 4b,d, showing a higher precision σ_D^{seg} in case of larger values of N_f. These results therefore highlight the importance of understanding how a large number of frames per subtrajectory N_f impacts the

precision of the MSD analysis within the context of fNTA, which has direct implications on potential experiments involving dynamic size change of specimen.

In the following section, the segmented MSD analysis is used to unlock the dependence of the determined hydrodynamic diameter of the nanosphere and the related error on the length of the segment (i.e., on different values of N_f). Specifically, the result of fitting the histograms shown in the right-handed plots of Figure 4 is statistically averaged, yielding the average nanosphere diameter as a function of N_f, $\bar{d}_h^{seg} = \bar{d}_h^{seg}(N_f)$ and the associated relative standard deviation of the free diffusion coefficient $\delta\sigma_D^{seg} = \sigma_D^{seg}/\overline{D_c^{seg}}$. This procedure was repeatedly conducted for various values of the number of frames per sub-trajectory within the interval $10^2 \leq N_f \leq 10^5$. Note that the resulting quantities include the properties of "one single" nano-object in case of different analysis conditions. This differs from quantities that characterize a large set of particles, as it is the case for Zetasizer measurements. The resulting distribution of the hydrodynamic diameters shows a stable averaged value of $\bar{d}_h^{seg} = 53$ nm (**Figure 5**a), whereas the associated relative error (error bar in Figure 5a) decreases with the number of frames per segment N_f, which is in qualitative accordance with Equation (2).

To understand the behavior of the error in greater detail, the relation between the standard deviation of the segmented diffusion coefficient $\delta\sigma_D^{seg}$ and N_f is compared in Figure 5b with values from simulations and forms the theoretical CRLB obtained from Equation (2). The experimental values of $\delta\sigma_D^{seg}$ are in good agreement with theoretical prediction down to $N_f = 10^3$, whereas at higher N_f values the experimental results deviate from the CRLB curve. This behavior can be attributed to the fact that the number of samples used in the statistical analysis to retrieve $\delta\sigma_D^{seg}$ (N_t/N_f) decreases as N_f increases, so that the statistical significance is reduced, correspondingly leading to a fluctuation of the values in the vicinity of the CRLB curve. To confirm this effect, we conduct 5000 simulations and averaged them (green curves in Figure 5b) to reach a situation with substantially higher statistical
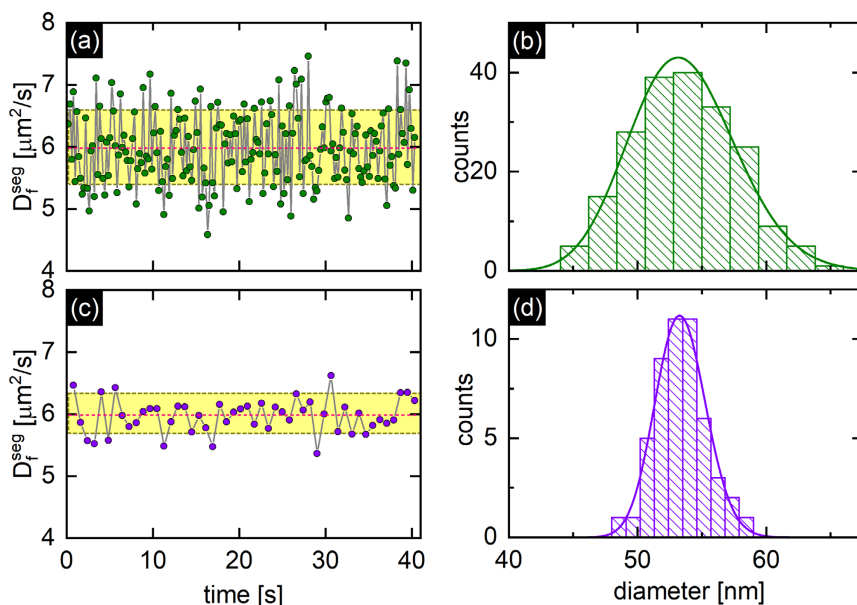
Figure 4. The segmented MSD analysis of the representative trajectory demonstrated by different segmentation examples (top row ((a)–(b)): no. frames per subtrajectory $N_f = 500$, ($N_s = 200$); bottom row ((c)–(d)): no. frames per subtrajectory $N_f = 2000$ ($N_s = 50$)). The plots on the left show the segmented free diffusion coefficient D_f^{seg} as a function of time, with the horizontal magenta line showing the average segmented free diffusion coefficient $\overline{D}_f^{seg}$ and the yellow area referring to the error margin within the interval of the first standard deviation ($\overline{D}_C^{seg} \pm \sigma_D^{seg}$), where $\sigma_D^{seg} = 0.58 \, \mu m^2 \, s^{-1}$ and $\sigma_D^{seg} = 0.28 \, \mu m^2 \, s^{-1}$ for $N_f = 500$ and $N_f = 2000$, respectively. The plots on the right show the corresponding histograms of the hydrodynamic diameters (hindrance corrected) with $\sigma_d^{seg} = 4.13 \, nm$ for $N_f = 500$ and $\sigma_d^{seg} = 1.97 \, nm$ for $N_f = 2000$, respectively, obtained from inverse Gaussian fitting (solid lines).
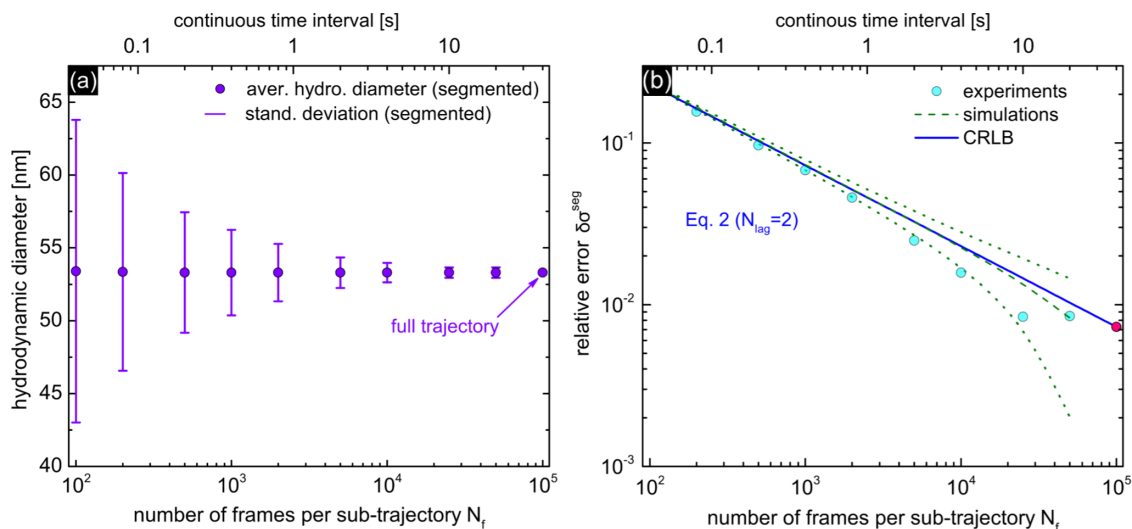

Figure 5. Statistical results of the segmented MSD analysis considering the representative trajectory shown in Figure 1d. a) Averaged hydrodynamic diameter (points) and associated standard error (lines) determined at discrete number of frames per subtrajectory N_f. The rightest point refers to the full trajectory ($N_f = 10^5$) and thus includes no error bars. b) Relative standard deviation of the segmented diffusion coefficient $\delta\sigma_D^{seg}$ as a function of N_f (bottom axis) and continuous time interval (i.e., number of frames per subtrajectory, top axis) for analyzed trajectory. The experimentally obtained errors are indicated by cyan points. The green lines refer to the simulated results (dashed line: mean error value; dotted lines: corresponding standard deviation from the mean value). The theoretical limit defined by Equation (2) is represented by the blue continuous line. The pink point at $N_f = 10^5$ predicts the relative error of the entire trajectory to $\delta\sigma_D^{seg}(N_f = N_t) = 0.7\%$ or $\sigma_D^{seg}(N_f = N_t) = 0.04 \, \mu m^2 \, s^{-1}$.

significance. Note that for a fixed value of N_f the single trajectory analyzed here yields a single value of $\delta\sigma_D^{seg}$ which fluctuates around the theoretical curve, whereas the results of the simulations include 5000 trajectories, each of which has been exposed to the segmented analysis, with the resulting averaged values (dashed green line in Figure 5b) following the CRLB behavior.

6. Discussion

One essential result of the segmented MSD analysis (Figure 5b) is an experimentally determined correlation between the precision of the diffusion coefficient determination and the number of frames per subtrajectory, $\delta\sigma_D^{seg} = \delta\sigma_D^{seg}(N_f)$. This dependency allows adapting a potential experimental configuration with respect to the precision of the diameter that needs to be determined. For instance, if a diffusion coefficient or diameter shall be measured with a relative error of 5%, each subtrajectory needs at least $N_f = 1100$ frames.

The dependency $\delta\sigma_D^{seg} = \delta\sigma_D^{seg}(N_f)$ is essential in case fNTA is used for analyzing dynamic processes, as the number of frames per subtrajectory can be directly transferred into a continuous time interval that can be used via the frame rate $\Delta T = N_f/\nu$ (top axes in Figure 5a,b). For instance, if a time interval of 1 s is required, the relative error with respect to the diffusing coefficient is about 4% for the frame rate used here. Note that the time interval ΔT is always related to the frame rate that is used in the specific experiments. Long time intervals can be obviously achieved for low frame rates, whereas, however, high statistical significance cannot be reached in such experiments due to a low number of frames per time interval.

To place the achieved results in the context of other approaches, **Table 1** shows several key parameters of reported NTA experiments. While other experiments have reached similar tracks length of the order of 10^5, our approach uniquely combines this with a precise analysis of a fast diffusion process (i.e., a large diffusion coefficient)—a feature that essentially results from the confinement of the nano-object to the nanofluidic channel. Note that for the experimental situation considered here the free diffusion length (distance over which the particle can diffuse before it is lost) is 22 µm at kHz frame rates, exceeding most of the other experiments shown in Table 1. This unique property is particularly visible when the combination of the columns "frame rate" and "calculated D" is considered. To emphasize the benefit of having the transverse confinement, the combinations of diffusion coefficient and number of acquired
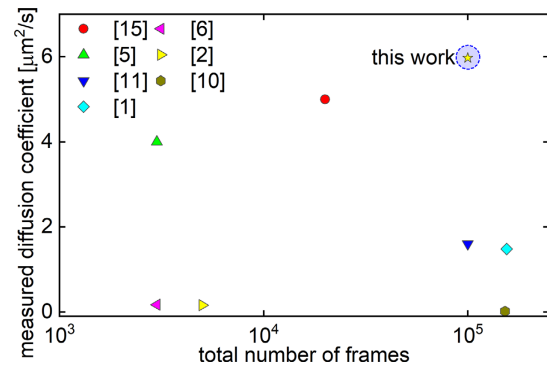

Figure 6. Diffusion coefficient versus total number of frames for various reported nanoparticle tracking experiments (according to Table 1). The yellow star inside the blue circle indicates the results achieved in this work.

frames of the experiments shown in Table 1 are shown in **Figure 6**. We would like to again emphasize that a fast acquisition of a large number of data points enables both 1) evaluating the entire trajectory and retrieving the diameter via MSD analysis with high accuracy and 2) cutting the trajectory into segments and evaluating each trajectory individually, thus allowing for time-resolved diameter analysis.

The number of frames of the representative trajectory shown in Figure 1d is $N_f = 10^5$, which is the approximate number of frames that can be continuously recorded with the current setup configuration. This value mainly results from the extension of our FoV of our imaging system along the longitudinal direction having a length of $L_{FoV} = 100$ µm. Within the recording time ($t_{rec} = 40$ s), the nanosphere has an expected diffusion length of $L_{div} = \sqrt{2D_c t_{rec}} \approx 22$ µm (defining the maximal length when the particle diffuses in one direction along the fiber), which is about five times shorter than L_{FoV}, yielding a very high probability that the object remains in the FoV during measurement. Note that recording time was selected based on experience. Further increase of the number of frames for maintaining the situation of having a high diffusion coefficient can be achieved by a camera

Table 1. Key benchmark figures of reported nanoparticle tracking experiments. The values in brackets refer to the corresponding free diffusion coefficients calculated via the Einstein−Stokes relation. The column "calculated D (50 nm)" refers to the free diffusion coefficient of a 50 nm nanoparticle using the respective viscosity value, therefore allowing for a direct comparison of the different diffusion scenarios.

Particle/ diameter [nm]	Measured $D*$ [µm² s⁻¹]	Calculated viscosity[a] [Pa s]	Calculated D[b] (50 nm) [µm² s⁻¹]	Frame rate [Hz]	Frames/ duration [1]/[s]	Diffusion length[c] [µm]	Environment	Approach	Reference/ year
Au/50	5.97 (8.6)[d]	0.0014	5.97	2480	100 000/41	22	Water	Nanobore fiber	This work
Au/51	5 (8.4)[d]	0.0017	5.05	1000	20 000/20	14	Water	Nanobore fiber	[13]/2015
Au/100	≈4 (4.3)[d]	0.0011	7.81	25	3000/120	31	Water	Dark-field microscopy	[5]/2014
Au/20	≈1.6	0.0134	0.64	100 000	100 000/1	1.7	Membrane	iSCAT microscope	[11]/2014
Au/20	≈1.48	0.0145	0.59	50 000	155 000/3	3	Membrane	iSCAT microscope	[1]/2016
Fluo-beads/200	0.17	0.0126	0.68	20	3000/150	7.14	Glycerol–water	Multifocal microscopy	[6]/2019
Au/20	≈0.16	0.1342	0.064	1000	5000/5	1.26	Membrane	iSCAT microscope	[2]/2014
Fluo-beads/20	0.017	1.2731	0.0068	250	152 000/608	4.5	Glycerol	Fluo-microscope	[10]/2013

[a]Calculated viscosity $\eta* = k_B T/3\pi D* d$; [b]Calculated diffusion coefficient of 50 nm particle using the viscosity $\eta*$; [c]$l = \sqrt{2D*t}$, t is the recording time; [d]The ones in brackets are the free diffusion coefficients of the related particles in water, using Stokes−Einstein relation.

with a larger chip. For instance, Basler cameras can have chips with 4000 pixels instead of 1000 used in the current experiments, leading to a 4 times larger area and consequently to 16 times longer observation time. Moreover, establishing a lower resolution by lowering magnification increases the FoV accordingly, leading to longer observation time. Note that the presented fiber-based NTA system can be straightforwardly applied to dielectric nano-objects such as viruses or vesicles, suggesting significant relevance of the results achieved within the context of bioanalysis. A possible extension of the results presented here is represented by applying electric field, while observing the object under investigation,[26,34] representing an interesting future direction toward measuring, for example, electrophoretic mobility, as suggested by first experiments.[16]

7. Conclusion

NTA represents one essential technology to characterize the motion of diffusing nano-scale objects with applications in fields such as bioanalytics, microrheology, and nano-object characterization in general. Here, the analysis of dynamic processes and high-precision measurements requires tracks with thousands of frames to reach high statistical significance, ideally at high frame rates. In this work, we successfully demonstrate that NBF-based NTA allows for acquiring trajectories of fast diffusion nano-objects with hundred thousand frames at kHz frame rates. The essential feature of this concept is the inclusion of a nanofluidic channel in the centre of a doped core step index fiber. This geometry confines the diffusion of the nano-objects to the observation region by preventing transverse diffusion and allows to record the Brownian motion of the object over extraordinary long time scales via microscopically detecting the elastically scattered light. The benefits of the concept are discussed on a representative track of a gold nanosphere (diameter: 53 nm) diffusing in water in over nearly 10^5 frames, recorded at frame rates of more than $2\,\text{kHz}$ at a diffusion constant of $6\,\mu\text{m}^2\,\text{s}^{-1}$. MSD and PSD analyses are both in excellent agreement with expectations justifying the NBF-based NTA approach. A segmented MSD analysis reveals an unambiguous correlation between the precision of determined diameter and continuous time interval (i.e., number of frames per subtrajectory) that is in line with theory. The results are placed in the context of reported works, showing that NBF-based NTA uniquely provides the opportunity to acquire tracks with thousands of frames of fast-diffusing nano-objects exceeding the capabilities of current systems.

The presented results demonstrate the opportunities and limitations of using NBFs within the context of NTA with regard to analyzing the properties of single nano-objects. This provides a future pathway 1) for determining diameters with extraordinary high precision of single species and 2) monitoring dynamic processes of the object itself or of the fluidic environment, both of which are relevant within biology (living cell analysis[7]), microrheology,[35] and nano-object characterizations in general.

Supporting Information

Supporting Information is available from the Wiley Online Library or from the author.

[1] H. M. Wu, Y. H. Lin, T. C. Yen, C. L. Hsieh, *Sci. Rep.* **2016**, *6*, 20542.
[2] C. L. Hsieh, S. Spindler, J. Ehrig, V. Sandoghdar, *J. Phys. Chem. B* **2014**, *118*, 1545.
[3] M. J. Saxton, K. Jacobson, *Annu. Rev. Cell Dev. Biol.* **1997**, *26*, 373.
[4] K. M. Spillane, J. Ortega-Arroyo, G. de Wit, C. Eggeling, H. Ewers, M. I. Wallace, P. Kukura, *Nano Lett.* **2014**, *14*, 5390.
[5] C. Haiden, T. Wopelka, M. Jech, F. Keplinger, M. J. Vellekoop, *Langmuir* **2014**, *30*, 9607.
[6] X. Wang, H. Yi, I. Gdor, M. Hereld, N. F. Scherer, *Nano Lett.* **2019**, *19*, 6781.
[7] R. W. Taylor, R. G. Mahmoodabadi, V. Rauschenberger, A. Giessl, A. Schambony, V. Sandoghdar, *Nat. Photonics* **2019**, *13*, 480.
[8] R. Metzler, J. H. Jeon, A. G. Cherstvy, *BBA-Biomembranes* **2016**, *1858*, 2451.
[9] N. Granik, L. E. Weiss, E. Nehme, M. Levin, M. Chein, E. Perlson, Y. Roichman, Y. Shechtman, *Biophys. J.* **2019**, *117*, 185.
[10] D. Ernst, J. Köhler, *Phys. Chem. Chem. Phys.* **2013**, *15*, 845.
[11] Y.-H. Lin, W.-L. Chang, C.-L. Hsieh, *Opt. Express* **2014**, *22*, 9159.
[12] C. S. Xu, H. Cang, D. Montiel, H. Yang, *J. Phys. Chem. C* **2007**, *111*, 32.
[13] S. Faez, Y. Lahini, S. Weidlich, R. F. Garmann, K. Wondraczek, M. Zeisberger, M. A. Schmidt, M. Orrit, V. N. Manoharan, *ACS Nano* **2015**, *9*, 12349.
[14] S. Jiang, R. Förster, M. Plidschun, J. Kobelke, R. Fatobene Ando, M. A. Schmidt, *Nanophotonics* **2020**, *9*, 4545.
[15] R. Förster, S. Weidlich, M. Nissen, T. Wieduwilt, J. Kobelke, A. M. Goldfain, T. K. Chiang, R. F. Garmann, V. N. Manoharan, Y. Lahini, M. A. Schmidt, *ACS Sens.* **2020**, *5*, 879.
[16] S. Faez, S. Samin, D. Baasanjav, S. Weidlich, M. Schmidt, A. P. Mosk, *Faraday Discuss.* **2016**, *193*, 447.
[17] K. Schaarschmidt, S. Weidlich, D. Reul, M. A. Schmidt, *Opt. Lett.* **2018**, *43*, 4192.
[18] A. Tuniz, S. Weidlich, M. A. Schmidt, *Phys. Rev. Appl.* **2018**, *9*, 044012.
[19] S. Jiang, K. Schaarschmidt, S. Weidlich, M. A. Schmidt, *J. Light. Technol.* **2018**, *36*, 3970.

[20] X. Bian, C. Kim, G. E. Karniadakis, *Soft Matter* **2016**, *12*, 6331.

[21] D. B. Allan, T. Caswell, N. C. Keim, C. M. van de Wel, *soft-matter/trackpy: Trackpy v0.4.2, Zenodo*, https://doi.org/10.5281/zenodo.3492186 (accessed: October 2019).

[22] S. Faez, A. Carattino, A. Mosk, PyNTA: An Open Source Software Application for Live Particle Tracking. Preprints 2019, 2019060251, https://doi.org/10.20944/preprints201906.0251.v1.

[23] X. Michalet, A. J. Berglund, *Phys. Rev. E* **2012**, *85*, 061916.

[24] T. Benesch, S. Yiacoumi, C. Tsouris, *Phys. Rev. E* **2003**, *68*, 021401.

[25] S. Ghosh, N. Karedla, I. Gregor, *Lab Chip* **2020**, *20*, 3249.

[26] F. Ruggeri, F. Zosel, N. Mutter, M. Rozycka, M. Wojtas, A. Ozyhar, B. Schuler, M. Krishnan, *Nat. Nanotechnol.* **2017**, *12*, 488.

[27] J. J. L. Higdon, G. P. Muldowneyt, *J. Fluid Mech.* **1995**, *298*, 193.

[28] S. Zacks, *The Theory of Statistical Inference*, Wiley, New York **1971**.

[29] X. Michalet, *Phys. Rev. E* **2010**, *82*, 041914.

[30] A. J. Berglund, *Phys. Rev. E* **2010**, *82*, 011917.

[31] K. Berg-Sørensen, H. Flyvbjerg, *Rev. Sci. Instrum.* **2004**, *75*, 594.

[32] B. M. Lansdorp, O. A. Saleh, *Rev. Sci. Instrum.* **2012**, *83*, 025115.

[33] M. Plidschun, S. Weidlich, M. Šiler, K. Weber, T. Čižmár, M. A. Schmidt, *Opt. Express* **2019**, *27*, 36221.

[34] M. J. Skaug, C. Schwemmer, S. Fringes, C. D. Rawlings, A. W. Knoll, *Science* **2018**, *359*, 6383.

[35] T. Moschakis, *Curr. Opin. Colloid Interface Sci.* **2013**, *18*, 311.